Desalination and Water Treatment
www.deswater.com

doi: 10.5004/dwt.2019.23324

143 (2019) 333–351
March

Enhanced naproxen removal over magnetic quaternized dextrin ionomer: response surface optimization, kinetics, isotherm and comparing study

Fatemeh Shirkavand[a,b], Mostafa Hossein Beyki[b], Farzaneh Shemirani[b,*]

[a]*Alborz Campus, University of Tehran, Tehran, Iran, email: f.shirkavand@ut.ac.ir*
[b]*School of Chemistry, University College of Science, University of Tehran, Tehran, Iran, emails: shemiran@khayam.ut.ac.ir (F. Shemirani), hosseinbakim@gmail.com (M.H. Beyki)*

Received 28 April 2018; Accepted 18 October 2018

ABSTRACT

In this work, a green quaternized nanohybrid was selected to enhance naproxen removal from aqueous solution hence magnetic dextrin was synthesized by a simple one-step precipitation route and modified by covalently binding tributylamine on its surface. The nanohybrid was characterized with energy dispersive X-ray spectroscopy, X-ray diffraction, field emission scanning electron microscopy, vibrating sample magnetometry (VSM), Fourier transform infrared spectroscopy and N_2 adsorption–desorption techniques. Prepared hybrid showed a mesoporous nanostructure with a surface area of 46.1 m^2/g and pore diameter of 7.54 nm. Result for VSM analysis revealed that magnetic dextrin and ionomer have the Ms value of 46.27 and 24.9 emu/g, respectively, which made the nanohybrid a good candidate for magnetic adsorption process. Effective parameters on naproxen adsorption were optimized by response surface methodology using Box–Behnken design. Naproxen adsorption followed fast equilibrium time of 10 min at a pH of 8.0 and ionic strength of 8% by using 8 mg of the adsorbent. Kinetic study showed that adsorption onto both adsorbents followed pseudo-second-order model. Isotherm study was performed based on Langmuir and Freundlich models and results showed that the Freundlich model can better describe the adsorption process. The maximum adsorption capacity of magnetic dextrin and ionomer was 137 and 166.6 mg/g, respectively. This result revealed enhances in naproxen removal by using the ionomer which made it a good candidate for water treatment purpose.

Keywords: Adsorption; Drug removal; Magnetic ionomer; Naproxen; Response surface methodology

1. Introduction

Water is the essential substance for all life as an adequate supply of safe water is a fundamental right for human, animals, and plants. However, due to tremendous increases in industrialization in the last few decades, it is very difficult to obtain pure and safe water free from hazardous materials. In other words, reliable access to clean and affordable water is gradually becoming a major global challenge [1–3]. Because of various unplanned activities, surface waters and groundwater can be contaminated by various toxic and hazardous materials such as drugs and personal care products [4]. In recent decades, the possible environmental risks of the anti-inflammatory drugs to aquatic ecosystems have been raised since they are designed to be biologically active [5]. Among various pharmaceuticals belonging to the group of non-steroidal anti-inflammatory drugs (NSAIDs), naproxen with an aryl acetic acid group in its structure, is a synthetic one widely used to treat inflammation or pain in human beings. In its pure form, it has a log K_{ow} of 3.18, and a pKa of 4.15 which confirmed it is a relatively hydrophilic compound that can easily get into the aquatic media in a very fast and uncontrolled manner causing water and soil pollutions [6–8]. At the neutral pH media, the naproxen's are quite stable; however, they can be slowly cleaved only when are heated

* Corresponding author.

in concentrated sulfuric and nitric acids [9]. In this context, there is an increasing demand for competent methods to remove NSAIDs from water and wastewaters. Up to now, several physical and chemical strategies to remove emerging compounds from aqueous media have been proposed. Most employed methods for the removal of drugs include osmosis, coagulation–flocculation, biodegradation, electroflotation, advanced oxidation, ion exchange, and filtration [10–17]. Despite the benefit of the mentioned methods, they showed some specific shortcomings. It was found that sedimentation and coagulation processes are ineffective for the removal of naproxen. Moreover, the oxidation process generates intermediate compounds that in some cases are more toxic than their original compounds [18,19]. In other words, most employed techniques are energy intensive as well as require expensive equipment for their successful performances [20]. It can be noted that the process of adsorption is the most preferred method for removing drugs from aqueous solutions because it can be applied easily as well as the process efficiencies and the surface properties of adsorbents can be modified according to the adsorbate [21–23]. In recent years biosorbents have attracted a great deal of attention for the removal of micropollutants owing to their abundance in nature, inexpensive and environmentally benign characteristics [24,25]. Among various types of biosorbents, dextrin as an inexpensive non-toxic water-soluble polysaccharide is a useful biopolymer with a wide range of properties. It is a class of low molecular weight carbohydrates produced by hydrolysis of starch or glycogen which exhibits favorable biodegradability as can be used in food industry and in pharmaceutics as a binder, and diluent [26]. In the view of water treatment purpose, dextrin should be chemically modified to improve the surface area and active sites of it in order to render more remediation of water pollutants [27].

In recent years, ionic liquids (ILs) with the unique properties have attracted great interests as disposable coating material since their structure consists of bulky organic cations combined with inorganic or organic anions. They are considered as a green reaction media with unique properties such as low melting points, negligible vapor pressures and high thermal stability [28,29]. Despite the worthiness of ILs as advanced material, their employment is along with a main drawback, that is, the low feasibility of recycling. To overcome this issue, ILs can be immobilized on a solid matrix such as magnetic polymeric compounds which generates an efficient type of advanced material for separation purpose [30]. The magnetic IL-based adsorption process is a rapid and effective technique that is capable to treat aqueous solution within a short time with no contaminants [31–33].

Based on the mentioned remarks at above this work presents an efficient magnetic adsorption system for naproxen removal. γ - Fe_2O_3 – Dextrin nanoparticles were chemically modified by covalent attachment of tributylamine onto their surface. Epichlorohydrin (ECH) was used as a linker to attach tertiary amine to magnetic dextrin. Effective parameters on naproxen adsorption were optimized with the response surface method (RSM) using Box–Behnken design (BBD) in order to identify the most important parameters and their interactions. In comparison with one factor at a time design, by means of RSM, the experimental procedure can be simplified and the overall costs associated with the experiment decreased [34]. Kinetic and isotherm models were also studied and results were discussed and compared with magnetic dextrin and ILs based sorbent.

2. Experimental

2.1. Materials and instruments

Dextrin, $FeCl_2{\cdot}4H_2O$, sodium hydroxide, epichlorohydrin and butylamine were purchased from Merck Company (Darmstadt, Germany). Ethanol was supplied from Bidestan Company (Qazvin, Iran). The pH adjustment was performed with NH_3 and HCl solution (0.1 mol L^{-1}).

The prepared composite was characterized by powder X-ray diffraction analysis (XRD), Field emission scanning electron microscopy (FESEM), Fourier transform infrared spectroscopy (FT-IR), energy dispersive X-ray spectroscopy (EDX), vibrating sample magnetometry (VSM) and N_2 adsorption–desorption measurements. XRD was recorded with powder diffractometer X' Pert MPD (Philips, Eindhoven Poland) using Cu-Kα radiation at λ = 1.540589 Å. FESEM and EDX are carried out using $MRIA_3$ TESCAN. FT-IR was measured with Equinox 55 (Bruker, Germany) at the wavenumber of 400–4,000 cm^{-1}. VSM was recorded with MDKFD instrument, Kashan, Iran. The N_2 adsorption–desorption isotherms were measured on Nova Station A system. A PerkinElmer LS 50 spectrofluorimeter (PerkinElmer USA) equipped with xenon discharge lamp and quartz cell was used to record fluorescence measurements. A digital pH meter (model 692, Metrohm, Herisau, Switzerland) was used for the pH adjustment.

2.2. Synthesis of magnetic dextrin

To prepare magnetic dextrin, 5.0 g of $FeCl_2.4H_2O$ was dissolved in 100 mL of distilled water, and then 2.0 g of dextrin was poured to the iron solution under magnetic stirring. After stirring for 10 min, 4.0 g of NaOH in 20 mL of distilled water was added to the mixture and was irradiated sonically at 60°C for 1 h. The obtained black precipitate was filtered, washed with distilled water for five times and ethanol once then dried at 70°C for 5 h. At the synthesis process of magnetic dextrin, Fe^{2+} ions precipitates as $Fe(OH)_2$ then convert to Fe_2O_3 in contact with air. By using sonication, high temperatures and pressures are produced in the inner environment of the collapsing bubble and between the cavitation bubbles and bulk solution, causing the pyrolysis of water into H and OH radicals [35]. This situation accelerates the oxidizing of Fe^{2+} ions and facilitates the formation of Fe_2O_3 nanoparticles. The reactions during this synthetic process are summarized as follows:

$$Fe^{2+} + 2OH^- \rightarrow Fe(OH)_2 \quad (1)$$

$$H_2O \rightarrow H\cdot + OH\cdot \quad (2)$$

$$H\cdot + O_2 \rightarrow \cdot OOH \quad (3)$$

$$2\cdot OOH \rightarrow H_2O_2 + O_2 \quad (4)$$

$$2Fe(OH)_2 + H_2O_2 \rightarrow Fe_2O_3 + 3H_2O \quad (5)$$

2.3. Preparation of polymeric IL

Magnetic dextrin (1.0 g) was stirred in 50 mL of NaOH solution (0.2 mol L^{-1}) for 2 h then, 8.0 mL of ECH was added to the suspension and refluxed at 40°C for 6 h. Obtained mass was collected with the external magnetic field, washed with water once and ethanol three times, and then ultrasonically dispersed at 50 mL of ethanol for 10 min. After addition of 3.0 mL of butylamine, the mixture was refluxed at 70°C for 24 h along with stirring. After cooling to room temperature, the product was collected magnetically, washed with ethanol and distilled water and dried at 50°C for 4 h.

2.4. Optimizing effective parameter on naproxen adsorption

To evaluate effective parameters on naproxen adsorption, RSM was used. In fact, RSM is a group of empirical techniques used for optimizing variables to reach a maximum desired response [36]. BBD was used to run adsorption experiments by Design-Expert software version 7.0.0. The design consists of four factors including solution pH (*A*), contact time (*B*), adsorbent dose (*C*) and ionic strength (*D*), and removal percentage (%*R*) as a response. The experimental design consisted of a total of 29 runs, one block and five center point. Analysis of variance (ANOVA) was used to validate the equations; moreover, 3D response surface plots were drawn from the experimental data to overview the variables effects and optimum level of parameters. Drug sample volume and concentrations were 10 mL and 10 mg L^{-1}, respectively. Isotherm and kinetic studies were performed under optimum conditions for different concentrations of naproxen (10 mg L^{-1} for kinetic study and 5–150 mg L^{-1} for isotherm study) in 20 mL volumetric flasks. The pH and ionic strength of the solutions were adjusted to 8 and 8%. Then, 8 mg of the sorbent was added to each flask. After shaking for 10 min, the solid mass was separated and the concentration of the target analyte in the supernatant was determined by spectrofluorimeter. Removal percentage (%*R*) was calculated using the following equation:

$$\%R = 100 \times (C_0 - C_e)/C_0 \quad (6)$$

In this equation, C_0 and C_e (mg L^{-1}) represent initial concentration and remaining naproxen in the solution after equilibrium, respectively.

3. Results and discussion

3.1. Characterization

The crystallinity of the magnetic nanocomposite after and before IL immobilization was studied by XRD analysis (Fig. 1(a)). The characteristic peaks due to the iron oxide phase show scattering at 2θ°= 30.26, 35.34, 43.22, 53.55, 57.23 and 63.32 corresponding to the (220), (311), (400), (422), (511) and (440) planes of Fe_2O_3 crystal that match well with the standard spectra (00-003-0863.CAF). The XRD was dominant with the main peaks of magnetic nanoparticles which confirmed that the coating of nanoparticles with the dextrin resulted in a low effect on its crystallization. Moreover, the composite material exhibits one broad shoulder at around 2θ° = 6–20 that is assigned to the presence of dextrin on the magnetic nanoparticle structure [37]. After immobilization of IL, the pattern showed a low intensity of Fe_2O_3 peaks which was assigned to the dilution effect or the presence of the quaternized fragment on the nanoparticle surface which concealed the diffraction peaks of the nanoparticles and decreased the peaks intensity. From the XRD pattern, an average crystallite size of 11.2 nm was determined from the X-ray line broadening using the Scherrer equation:

$$D = 0.9\lambda/(\beta \cos\theta) \quad (7)$$

where D is the average crystallite size, λ (0.154 nm) is the X-ray wavelength used, β is the angular line width of half maximum intensity in radians (0.013) and θ is Bragg's angle expressed in degrees (18.05).

The results of EDX elemental analysis of the magnetic dextrin and ionomer are illustrated in Figs. 1(b) and (c). The spectra showed all expected component of the nanocomposite as it shows iron, carbon, oxygen, nitrogen and chlorine. The weight percentage of the mentioned elements is according to Table 1. Iron, carbon and oxygen are from magnetic nanoparticles and dextrin structure. Presence of chlorine and nitrogen in the EDX spectra is assigned to the ionomer on the magnetic dextrin surface. These observations strongly confirm the successful synthesis of the ionomer.

The VSM analysis was used to study the magnetic behavior of the nanocomposite and ionomer. The magnetic hysteresis loops are based on the magnetization, *M*, vs. the applied magnetic field, *H*. As can be seen in Fig. 2(a), the prepared magnetic dextrin has exhibited a clear hysteresis behavior with the magnetic parameters including saturation magnetization (Ms: 46.27 emu/g), coercivity (Hc: 21.52 Oe) and remnant magnetization (Mr: 1.95 emu/g). The value of the Ms for the synthesized magnetic dextrin is lower than naked magnetite nanoparticles reported in the literature (70 emu/g) [38] owing to disorder in magnetic moment orientation in the particles. In other words, magnetic nanoparticles have two sub-lattices sites in their structure which have been separated by oxygen atoms and Fe^{2+} and Fe^{3+} ions coexist in the two sub-lattices. Increase the occupation ratio of Fe^{3+} ions at the octahedral sites can lead to a decrease in the net magnetic moment [39]. Moreover, it is known that the contribution of the coating layers, as well as the volume fraction of the magnetic nanoparticles, has the main effect on the total magnetization [40]. The value of Ms for the ionomer was 24.89 emu/g which is lower than the Ms value of the magnetic dextrin. This can be attributed to the disaffiliation of the IL on the total magnetization along with a low volume fraction of the nanoparticles onto the final composite structure. The Mr and Hc of the ionomer were 0.6 emu/g and 24.95 Oe, respectively. The ratio of Mr/Ms is 0.042 and 0.024 for magnetic dextrin and ionomer which is between 0 and 1, therefore, it can be concluded that the magnetic materials have paramagnetic property [41].

The FT-IR spectra of magnetic dextrin, as well as ionomer, are shown in Fig. 2(b). The spectrum of the appeared materials shows transmittance owing to the stretching vibration of free and hydrogen bonded O–H at 3,000–3,700 cm^{-1}. Moreover, the C–H stretching, C–O stretching and the OH bending vibration of primary alcoholic groups and adsorbed water could be observed at 2,915; 1,036; 1,350 and

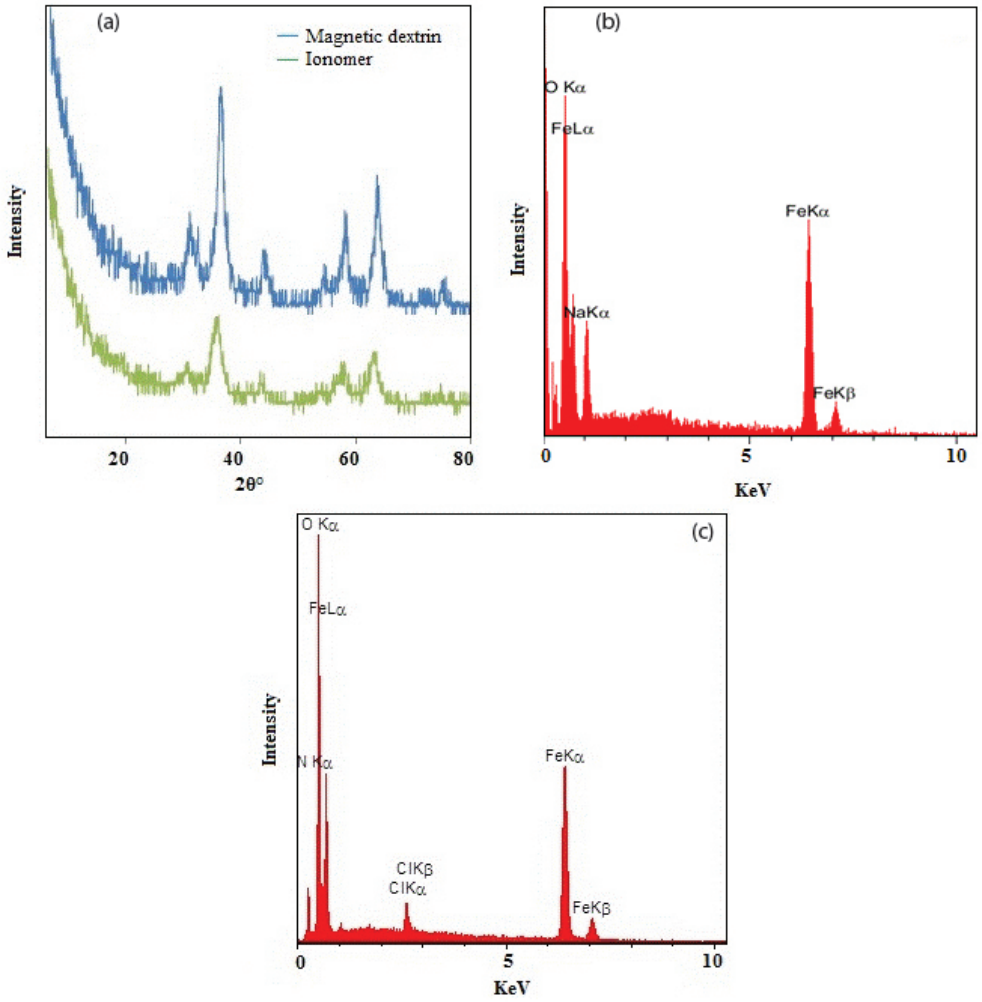

Fig. 1. XRD pattern of ionomer (a) and EDX spectra of magnetic dextrin and ionomer (b) and (c).

Table 1
EDX elemental analysis data of magnetic dextrin and ionomer

Elements	Percentage in ionomer	Percentage in magnetic dextrin
Fe	34.1	46.61
C	10.18	16.85
O	49.9	36.74
N	1.51	–
Cl	3.68	–

1,600 cm^{-1}, respectively [42]. The absorption peaks at 1,459 and 1,120 cm^{-1} relate to the CH_2 symmetric scissoring and C–O–C vibration, respectively. The spectrum of the ionomer is the same as the magnetic dextrin. According to the pattern, the C–O stretching and the OH vibration of primary alcoholic groups showed a decrease in the peak intensity. This can be assigned to the chemical bonding of hydroxyl groups of dextrin with an IL which causes hydroxyl groups to be in a rigid state with low vibration domain [43].

Fig. 3 showed the FESEM images of the magnetic dextrin and ionomer. The image indicated that the nanocomposite exhibited some bundles with an aggregated sphere-like structure. The aggregated structures are composed of nanoscale particles. Agglomeration is owing to the intramolecular hydrogen bonds of dextrin chain as well as the hydrophobic interaction between methylene groups of tertiary amine chain which provide the stiffness of the ionomer. In other words, the nanocomposite organizes in a rather complex fashion where an extended intra- and intermolecular network interaction is indicated as the basis of cohesion between the nanoparticles.

The N_2 adsorption–desorption isotherm for the magnetic dextrin and ionomer as well as corresponding Barrett, Joyner and Halenda pore size distribution curve is shown in Figs. 4(a) and (b). As can be seen, the curve show type II isotherm with a minor hysteresis loop as a result of filling and emptying of the mesopores by capillary condensation [44]. This type of isotherm illustrates slit-shaped pores with parallel walls. The BET surface area and pore size values are illustrated in Table 2. As can be seen after preparing ionomer surface area and pore volume increased. Moreover, the pore means the diameter of the material is 8.033 and 7.540 nm. According to the pore-size distribution, the materials are classified as mesopores compounds [45].

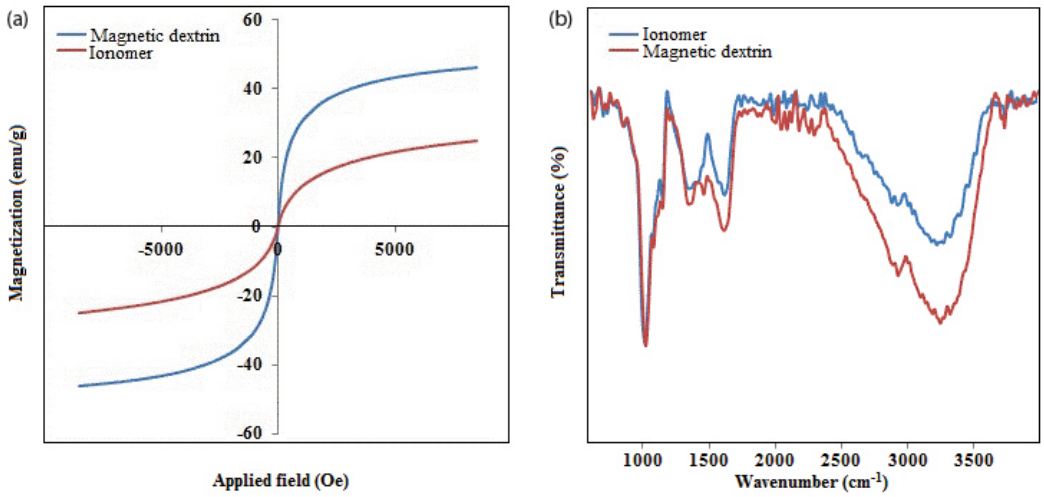

Fig. 2. VSM graph (a) and FT-IR spectra (b) of magnetic dextrin and ionomer.

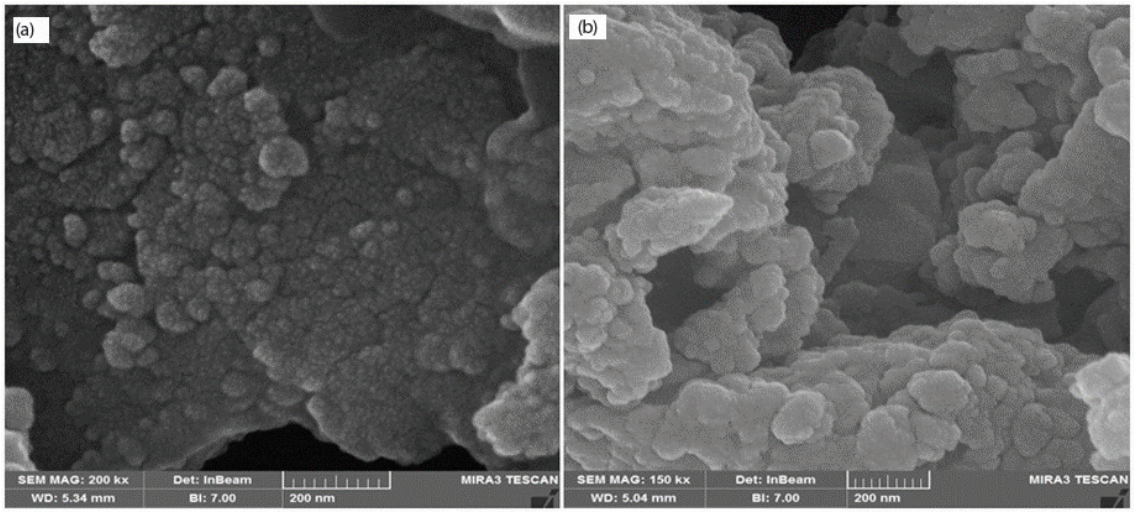

Fig. 3. FESEM image of magnetic dextrin (a) and ionomer (b).

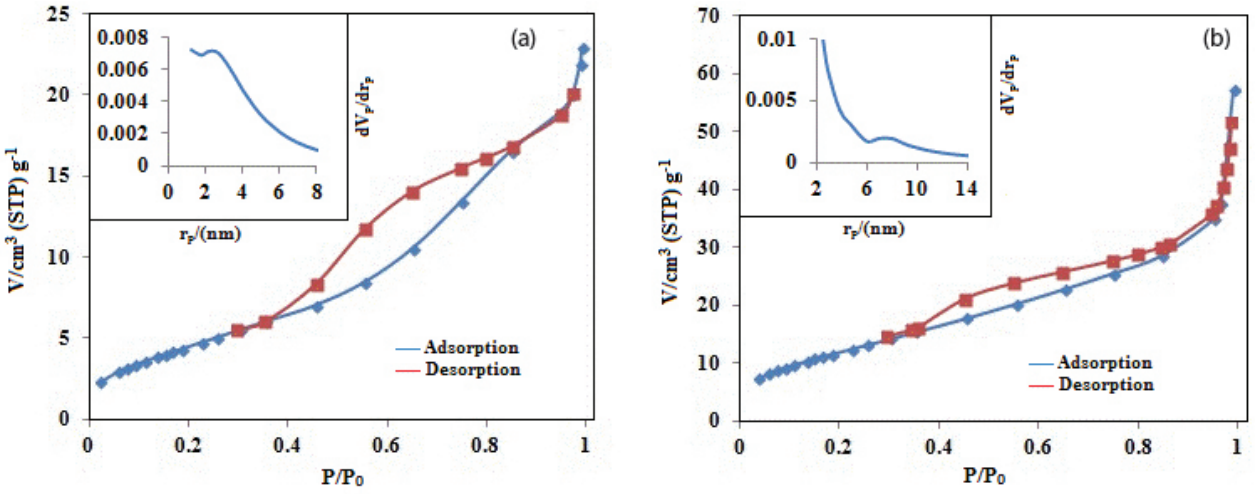

Fig. 4. N_2 adsorption–desorption and the pore size distribution of magnetic dextrin (a) and ionomer (b).

3.2. Fitting of process models

Four important variables on naproxen adsorption were optimized with BBD method. The variables and their studied range are shown in Table 3. Moreover, the BBD was performed at 29 runs in one block and the removal percentage was selected as a response. The design matrix and experimental results of naproxen removal by magnetic dextrin and ionomer are shown in Tables 4 and 5, respectively. The regression coefficients for the developed model were calculated and

Table 2
BET surface area data of magnetic dextrin and ionomer

Parameters	Magnetic dextrin	Ionomer
$a_{s,BET}$ ($m^2\ g^{-1}$)	17.27	46.10
Total pore volume ($cm^3\ g^{-1}$)	0.034	0.086
Mean pore diameter (nm)	8.033	7.540

Table 3
Experimental ranges levels and independent variables for naproxen removal by magnetic dextrin and ionomer

Variable	–1 level	+1 level
pH	3	9
Time	1	15
Dosage	5	20
Ionic strength	1	10

Table 4
Design matrix and experimental results of naproxen removal by magnetic dextrin

Run	Block	A: pH	B: time	C: dosage	D: ionic strength	Removal (%)
1	Block 1	6	1	12.5	10	43
2	Block 1	6	1	5	5.5	42
3	Block 1	6	8	12.5	5.5	7
4	Block 1	9	8	5	5.5	60
5	Block 1	3	1	12.5	5.5	3
6	Block 1	6	15	12.5	1	17
7	Block 1	6	8	12.5	5.5	1
8	Block 1	6	1	12.5	1	33
9	Block 1	9	15	12.5	5.5	62
10	Block 1	6	8	20	10	45
11	Block 1	3	8	5	5.5	20
12	Block 1	3	8	20	5.5	30
13	Block 1	6	8	12.5	5.5	11
14	Block 1	3	8	12.5	10	34
15	Block 1	6	8	5	1	21
16	Block 1	6	15	12.5	10	37
17	Block 1	6	8	12.5	5.5	20
18	Block 1	3	8	12.5	1	8
19	Block 1	6	8	5	10	35
20	Block 1	6	8	12.5	5.5	20
21	Block 1	9	8	20	5.5	62
22	Block 1	9	8	12.5	1	55
23	Block 1	9	1	12.5	5.5	60
24	Block 1	6	1	20	5.5	12
25	Block 1	6	15	5	5.5	1.2
26	Block 1	9	8	12.5	10	55
27	Block 1	6	15	20	5.5	50
28	Block 1	6	8	20	1	25
29	Block 1	3	15	12.5	5.5	15

Table 5
Design matrix and experimental results of naproxen removal by magnetic ionomer

Run	Block	A: pH	B: time	C: dosage	D: ionic strength	Removal (%)
1	Block 1	6	1	12.5	10	53.48
2	Block 1	6	1	5	5.5	52
3	Block 1	6	8	12.5	5.5	12
4	Block 1	9	8	5	5.5	75
5	Block 1	3	1	12.5	5.5	8
6	Block 1	6	15	12.5	1	22
7	Block 1	6	8	12.5	5.5	5.37
8	Block 1	6	1	12.5	1	43.89
9	Block 1	9	15	12.5	5.5	85
10	Block 1	6	8	20	10	58.28
11	Block 1	3	8	5	5.5	24.47
12	Block 1	3	8	20	5.5	39.16
13	Block 1	6	8	12.5	5.5	16.42
14	Block 1	3	8	12.5	10	44
15	Block 1	6	8	5	1	41.71
16	Block 1	6	15	12.5	10	47.96
17	Block 1	6	8	12.5	5.5	23
18	Block 1	3	8	12.5	1	12
19	Block 1	6	8	5	10	48.54
20	Block 1	6	8	12.5	5.5	25
21	Block 1	9	8	20	5.5	83
22	Block 1	9	8	12.5	1	62.65
23	Block 1	9	1	12.5	5.5	73
24	Block 1	6	1	20	5.5	18.16
25	Block 1	6	15	5	5.5	3.77
26	Block 1	9	8	12.5	10	85
27	Block 1	6	15	20	5.5	60
28	Block 1	6	8	20	1	45.59
29	Block 1	3	15	12.5	5.5	20.55

the empirical relationship between removal percentage (R%) and the variables was decoded. The equation is shown below:

$$\%\ \text{Removal} = 1{,}180 + 20.33A - 0.9B + 3.73C + 7.5D - 2.5AB - 2AC - 6.5AD + 19.7BC + 2.5BD + 1.5CD + 17.72A^2 + 6.62B^2 + 10.12C^2 + 10.72D^2 \quad (8)$$

$$\%\ \text{Removal} = 16.36 + 26.29A - 0.77B + 4.89C + 9.12D - 0.14AB - 1.67AC - 2.41AD + 22.52BC + 4.09BD + 1.46CD + 22.17A^2 + 6.66B^2 + 14.4C^2 + 16.32D^2 \quad (9)$$

At this equation, %R is the response (removal percentage); A, B, C and D are pH, contact time, sorbent dose and ionic strength as independent variables.

The significance of the coefficients was determined from F and p values from the ANOVA calculation in Tables 6 and 7. The regressions for the adsorption of naproxen onto magnetic dextrin and ionomer were statistically significant which is evident from the F values (13 and 13.9) with a low probability value ($p < 0.0001$). Based on the p-values of each model term, the independent variables (A and D), interactive coefficients (BC) and quadratic terms of A^2, C^2 and D^2) significantly affected the naproxen removal percentage. The value of R^2 (0.92 and 0.93 for magnetic dextrin and ionomer) was in good agreement with adjusted R^2 (0.85 and 0.86) and indicated a high dependence and correlation between the observed and the predicted values of response. The adequate precision of 10.66 and 11.9, which measures the signal to noise ratio, demonstrated the significance of the adsorption model since the ratio greater than 4 is desirable.

Table 6
ANOVA calculations for naproxen adsorption onto magnetic dextrin

Source	Sum of squares	df	Mean square	*F* value	*p*-value Prob > *F*	
Model	10,238.82	14	731.3443	13.01545	<0.0001	Significant
A-pH	4,961.333	1	4,961.333	88.29492	<0.0001	
B-time	9.72	1	9.72	0.172983	0.6838	
C-dosage	167.2533	1	167.2533	2.976542	0.1065	
D-ionic	675	1	675	12.01271	0.0038	
AB	25	1	25	0.444915	0.5156	
AC	16	1	16	0.284746	0.6020	
AD	169	1	169	3.007627	0.1048	
BC	1,552.36	1	1,552.36	27.62675	0.0001	
BD	25	1	25	0.444915	0.5156	
CD	9	1	9	0.160169	0.6950	
A^2	2,035.98	1	2,035.98	36.23355	<0.0001	
B^2	283.9802	1	283.9802	5.053885	0.0412	
C^2	663.8721	1	663.8721	11.81467	0.0040	
D^2	744.9532	1	744.9532	13.25764	0.0027	
Residual	786.6667	14	56.19048			
Lack of fit	511.8667	10	51.18667	0.745075	0.6796	Not significant
Pure error	274.8	4	68.7			
Corrected total	11,025.49	28				

Table 7
ANOVA calculations for naproxen adsorption onto magnetic ionomer

Source	Sum of square	df	Mean square	*F* value	*p*-value Prob > *F*	
Model	16,375.72	14	1,169.69	13.90	<0.0001	Significant
A-pH	8,293.44	1	8,293.44	98.58	<0.0001	
B-time	7.13	1	7.13	0.085	0.7752	
C-dosage	287.14	1	287.14	3.41	0.0859	
D-ionic	997.73	1	997.73	11.86	0.0040	
AB	0.076	1	0.076	8989E-004	0.9765	
AC	11.19	1	11.19	0.13	0.7208	
AD	23.28	1	23.28	0.28	0.6071	
BC	2,028.15	1	2,028.15	24.11	0.0002	
BD	66.99	1	66.99	0.80	0.3873	
CD	8.58	1	8.58	0.10	0.7541	
A^2	3,187.02	1	3,187.02	37.88	<0.0001	
B^2	288.01	1	288.01	3.42	0.0855	
C^2	1,344.52	1	1,344.52	15.98	0.0013	
D^2	1,728.63	1	1,728.63	20.55	0.0005	
Residual	1,177.81	14	84.13			
Lack of fit	919.27	10	91.93	1.42	0.3923	Not significant
Pure error	258.53	4	64.63			
Corrected total	17,553.53	28				

To check the validity of ANOVA, a normal distribution of residuals from the normal probability plot (NPP) was employed. The NPP explains the systematic departures from the assumptions that errors are normally distributed and independent of each other and the error variances are homogeneous [46]. The NPP is shown in Figs. 5(a) and 6(a). A straight line with low violation of the assumptions underlying the analysis, confirms the normality of the data. Perturbation plots in Figs. 5(b) and 6(b) show the comparative effects of all media components on the response. Based on the observed results a steep curvature in pH (*A*) and dosage (*C*) curve confirmed that the adsorption process is very sensitive to these factors. From the relatively flat line of the time (*B*) and ionic strength (*D*) can be concluded that the response is less sensitive to these variables. The relationship between the predicted value of the response (%*R*) with observed *R*% is shown in Figs. 5(c) and 6(c) and can be seen that most of the response points are located in a narrow range.

By taking removal percentage as the response, the 3D response surfaces (Figs. 7–10) indicate the effects of selected parameters on the removal of naproxen.

According to the results (from the 3D plots of pH vs. time, pH vs. dosage and pH vs, ionic strength at Figs. 7(a)–(c) and 8(a)–(c)), it can be seen that the removal percentage is very sensitive to pH since in the pH range from 3 to 9, mean removal efficiency was increased from about 15% to 85% and 5% to 62% by ionomer and magnetic dextrin, respectively. Contact time was designed in the range of 1–15 min. From the results (the 3D plots of pH vs. time, time vs. dosage and time vs. ionic strength at Figs. 7(a), 8(a), 9(a), 9(b), 10(a) and 10(b)), it can be seen that with increasing shacking time removal percentage was not changed significantly. This can be attributed to the external surface adsorption and absence of internal diffusion resistance. In fact, the functional groups on the ionomer surface easily interact with the functional groups of naproxen. In other words, fast equilibrium time could be assigned to the availability of various adsorption sites such as hydrophobic chain, ion exchanger fragments, hydrogen bonding sites and pores which ready to capture the target analyte [47].

Amount of adsorbent is the main factor which can affect the adsorption process. In other words, inefficient interaction

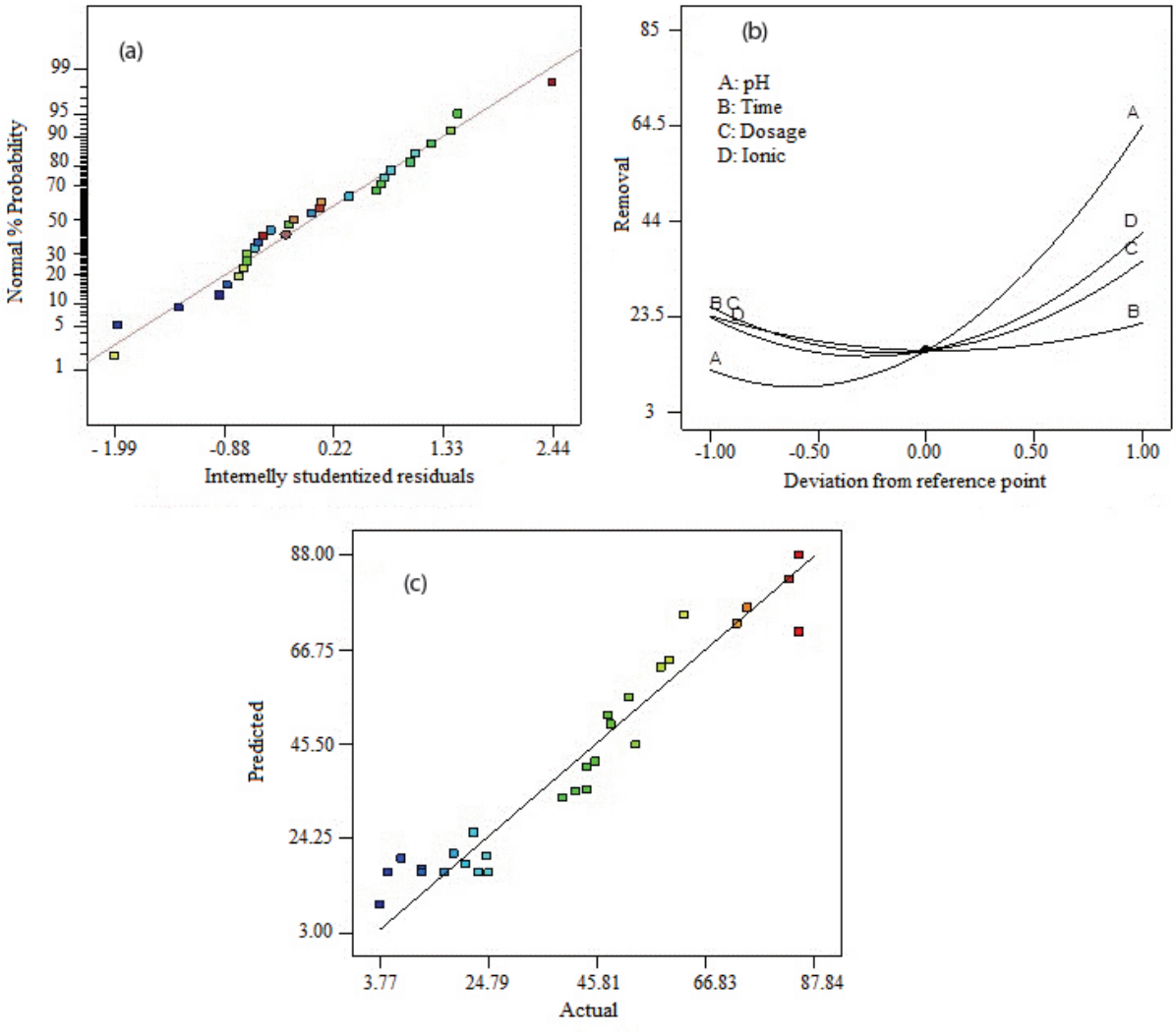

Fig. 5. NPP (a), perturbation (b) and predicted vs. actual responses (c) for naproxen adsorption onto magnetic ionomer.

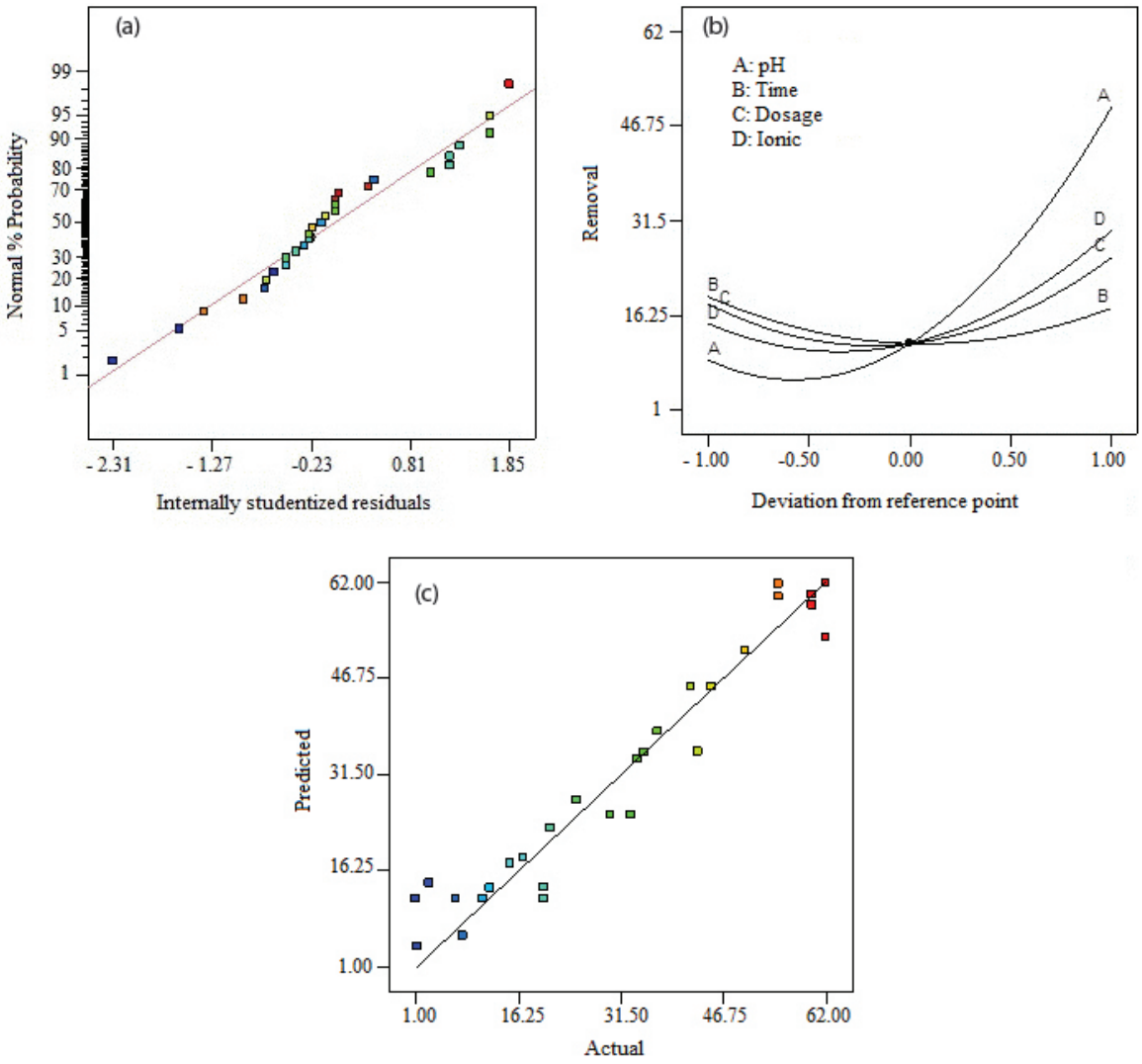

Fig. 6. NPP (a), perturbation (b) and predicted vs. actual responses (c) for naproxen adsorption onto magnetic dextrin.

at low adsorbent dosage causes low efficiency besides, high adsorbent dosage may cause overlapping of the adsorption sites which shield the binding sites from analyte [48]. Hence the amount of adsorbent was also selected as a variable and designed in the range of 5–20 mg. It is observed that the removal efficiencies increased very slowly as the dosages of sorbents increased which show availability of high binding sites and high active surface area on the sorbent surface.

The effect of ionic strength was studied in the range of 1.0%–10% (m/v). As shown in Figs. 7–10, adsorption of naproxen increased upon addition of $NaNO_3$ salt. Based on this observation, it can be concluded that attractive electrostatic forces are not the main adsorption mechanism for naproxen interaction with the adsorbent. In fact, at the first step adsorbate molecules adsorbs on the ionomer surface through ion exchange then could be stabilized by electrostatic attraction. In other words, salt ions induce some intermolecular forces such as van der Waals force; ion-dipole forces and dipole–dipole forces, causes dimerization of organic acids in the solution and aggregation of organic molecules which increase adsorption efficiency [49]. To evaluate the accuracy of the results obtained by the model, under optimum condition (Table 8), three experiments were carried out and results showed a good agreement between the optimum-calculated response (64% and 94%) and mean experimental response (65% and 93%).

3.3. Kinetic study

To quantify the changes in naproxen adsorption with time, four kinetic models including pseudo-first order, pseudo-second order, intraparticle diffusion and liquid film were selected. These models can be expressed by following equations:

$$\log(Q_e - Q_t) = \log Q_e - K_1 t \tag{10}$$

$$t/Q_t = 1/(K_2 Q_e^2) + (1/Q_e)t \tag{11}$$

$$Q_t = K_i t^{0.5} + C \tag{12}$$

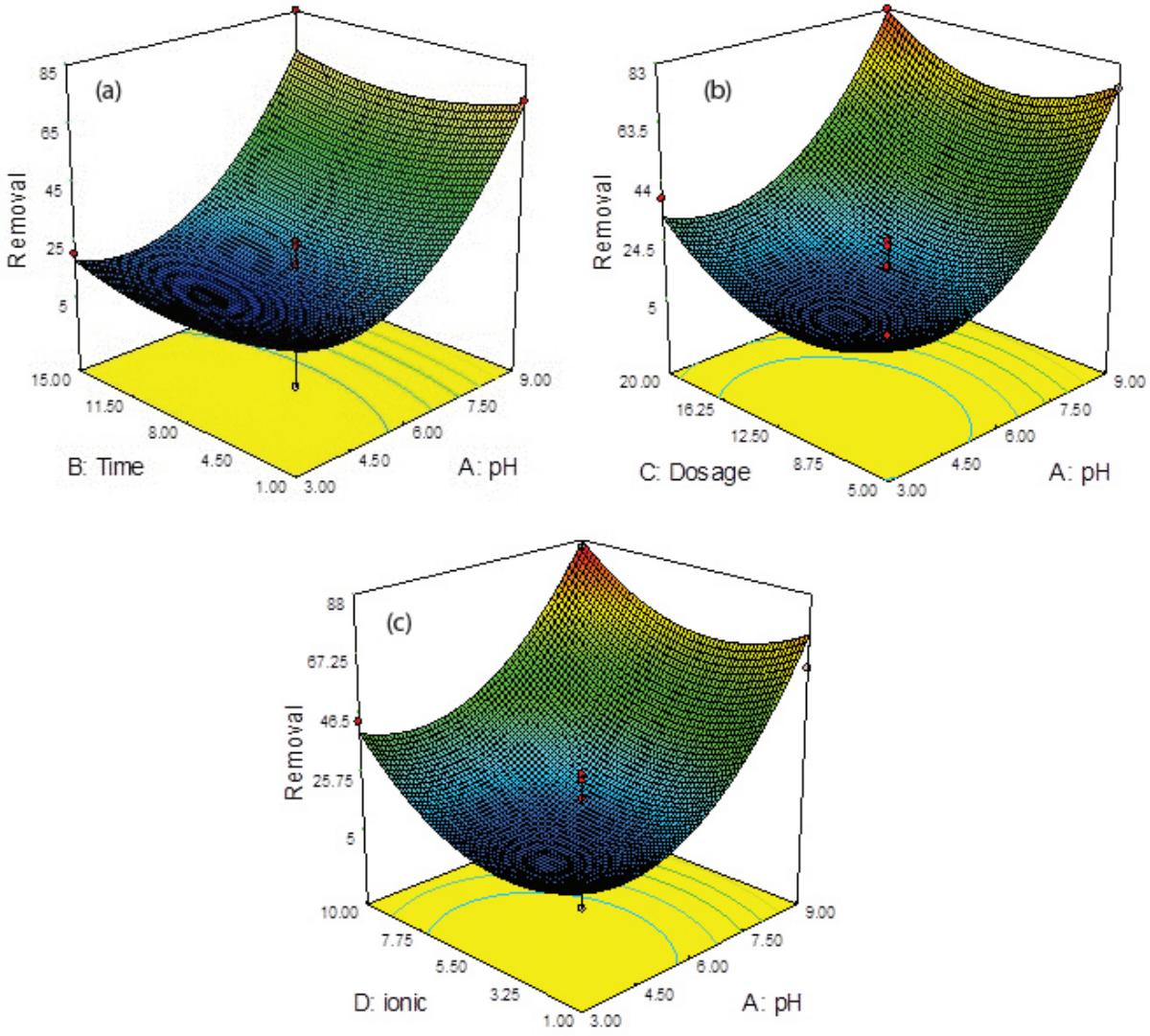

Fig. 7. 3D plots of pH vs. time (a), pH vs. dosage (b) and pH vs. ionic strength (c) for naproxen adsorption onto magnetic ionomer.

$$\ln(1 - F) = -K_{fd}t + C \quad (13)$$

in these equations, K_1, K_2, Q_e and Q_t are the pseudo-first-order adsorption rate constant (min^{-1}), the second-order rate constant (g mg^{-1} min^{-1}), the values of the amount adsorbed per unit mass at equilibrium and at any time t, respectively. Moreover, K_i and K_{fd} are the adsorption rate constants and F is the fractional attainment of equilibrium ($F = Q_t/Q_e$) [50,51]. Results of naproxen adsorption onto magnetic dextrin and ionomer are shown in Table 9. From the results, it can be seen that both Lagergren plot of pseudo-first-order model (Eq. (10)) and pseudo-second-order model (Eq. (11)) for naproxen adsorption by magnetic dextrin were linear while the value of Q_e based on second-order plot had a lower deviation with those obtained from the experimental data. Results also showed that only the pseudo-second-order model has high linearity and low Q_e deviation from the experimental data for naproxen adsorption by magnetic ionomer. This result confirmed that the pseudo-second-order kinetic model can better describe naproxen adsorption onto both adsorbents.

The intraparticle diffusion model (Eq. (12)) explains transport of analyte from the aqueous phase to the surface of adsorbent and subsequently diffuse into the interiors of the porous particles. This model was not linear for adsorption process with a high intercept which showed that the intraparticle diffusion was not the rate-limiting step. The liquid film diffusion model (Eq. (13)), explains the role of transport of the adsorbate from the liquid phase up to the solid phase boundary. It can be seen that the liquid film model of magnetic dextrin has good linearity. The small intercept value illustrated a role for the liquid phase, which transported the molecules to the sorbent surface in controlling the kinetic.

3.4. Isotherm study

In this study, adsorption equilibrium between the adsorbents amount and naproxen concentration was studied with Langmuir, Freundlich, Dubinin–Radushkevich (D–R) and Temkin models. The Freundlich model corresponded to a heterogeneous adsorption–complexation process whereas

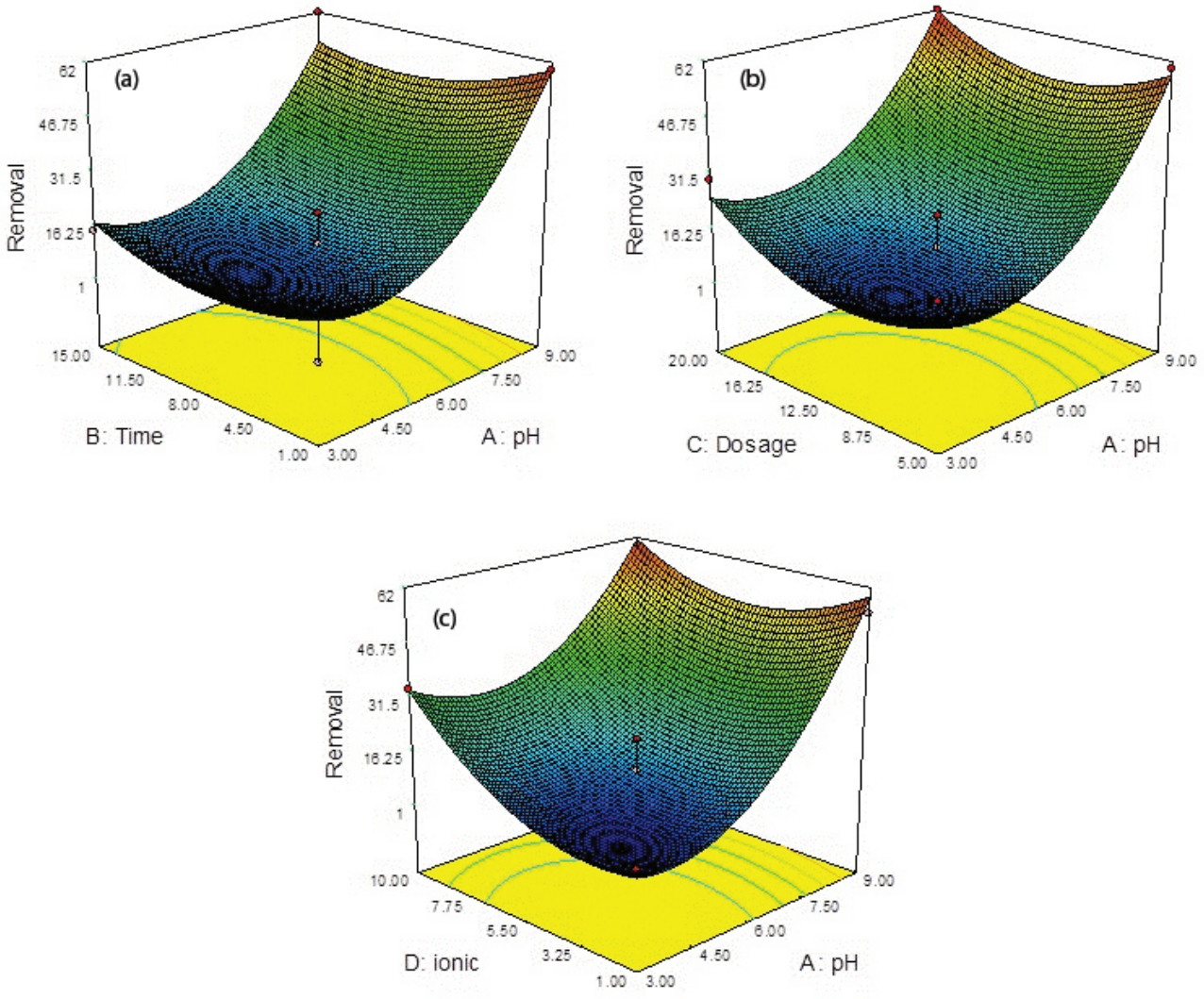

Fig. 8. 3D plots of pH vs. time (a), pH vs. dosage (b) and pH vs. ionic strength (c) for naproxen adsorption onto magnetic dextrin.

the Langmuir adsorption model describes a monolayer adsorption. The Langmuir model and the Freundlich models are shown as follows:

$$1/Q_e = 1/(C_e K_L Q_m) + 1/Q_m \quad (14)$$

$$\ln Q_e = \ln K_f + 1/n \ln C_e \quad (15)$$

At the Langmuir equation, Q_e is the amounts of naproxen sorbed per unit mass of the sorbent (mg g^{-1}), C_e is the concentration of naproxen in the liquid phase at equilibrium, Q_m and K_L are the adsorption capacity and the Langmuir coefficient, respectively [15,52]. The Freundlich coefficients which can be evaluated from the slopes and intercepts of $\ln Q_e$ vs. $\ln C_e$ are n and K_f. Dubinin–Radushkevich (D–R) and Temkin isotherm equations are shown in Eqs. (16) and (17):

$$\ln Q = \ln Q_{max} - \beta\varepsilon^2 \quad (16)$$

$$Q_e = B \ln A_T + B \ln C_e \quad (17)$$

where Q_e is the amount of analyte sorbed per unit mass of the sorbent and C_e is the amount of analyte in the liquid phase at equilibrium. The β is the activity coefficient related to sorption energy and ε is the Polanyi potential that can be calculated as follows:

$$\varepsilon = RT \ln(1 + 1/C_e) \quad (18)$$

In this equation, R is the gas constant (8.314 J /mol K) and T is the absolute temperature (K). The constant β is used to calculate mean sorption energy (E) by Eq. (19). E is defined as the free energy transfer of one mol of solute from the infinity of the surface of the sorbent.

$$E = 1/(2\beta)^{1/2} \quad (19)$$

Temkin model (Eq. (17)) assumes that heat of adsorption of all molecules in the layer would decrease linearly rather than logarithmic with coverage. At the equation A_T is Temkin isotherm equilibrium binding constant (L/g), R is universal

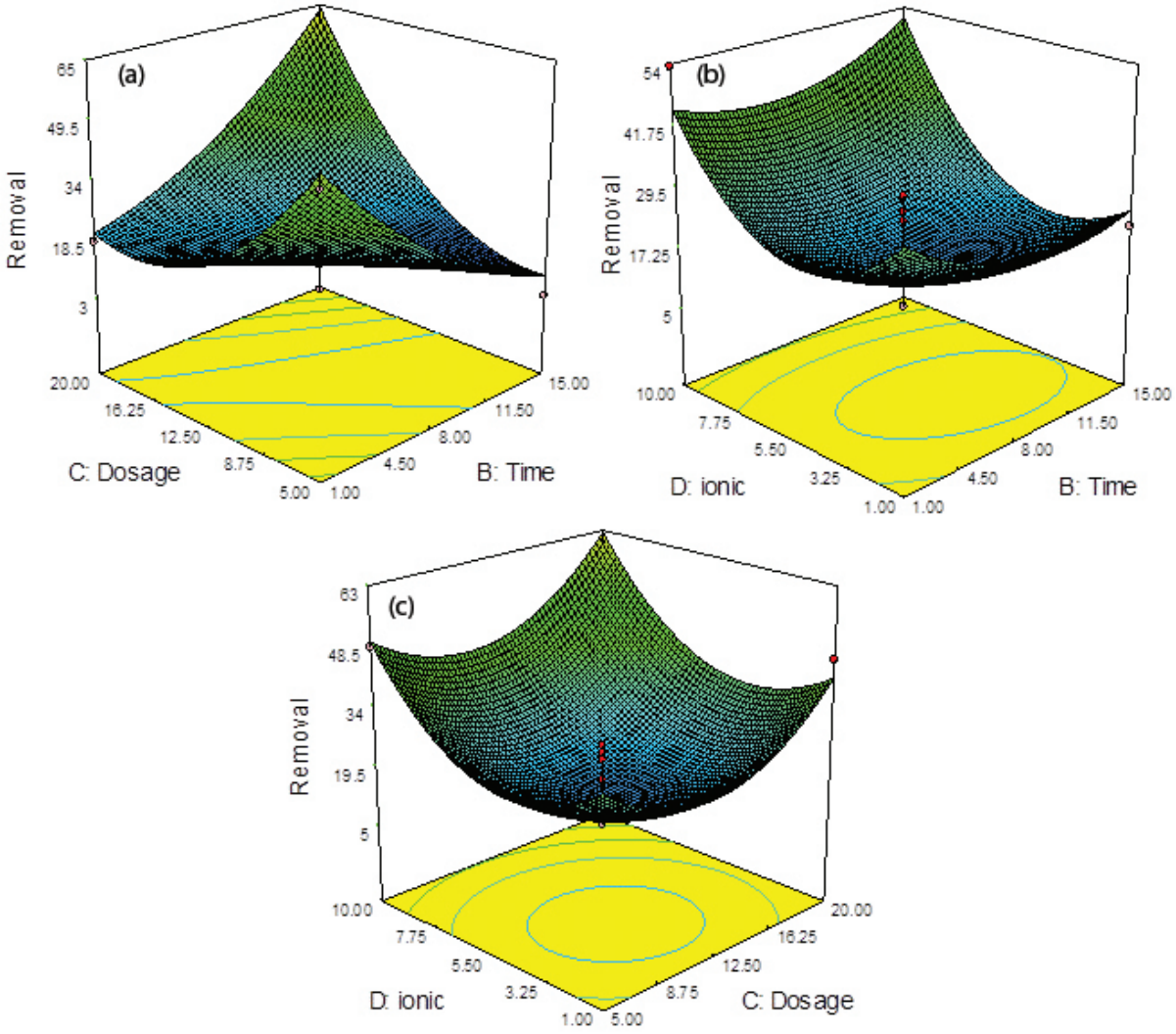

Fig. 9. 3D plots of dosage vs. time (a), ionic strength vs. time (b) and ionic strength vs. dosage (c) for naproxen removal by ionomer.

gas constant (8.314 J/mol/K), which represents the temperature at 298 K and B is constant related to the heat of sorption (J/mol) [53].

According to the results in Tables 10 and 11 as well as Figs. 11 and 12, both Langmuir and Freundlich isotherm models showed good linearity (higher than 0.9) however, D–R and Temkin models show low linearity.

It is not possible to select the best-fitted model based on the linear form of the equations. In other words, the linear form of the isotherm equation does not represent the errors in the isotherm curves. Therefore, RMSE (root mean square error) has studied with MATLAB R2013a software fit the equilibrium adsorption data. According to the results in Tables 11 and 12, the Freundlich isotherm model with lower RMSE value with respect to other models fitted better for naproxen adsorption [54]. The results for D–R model showed that the magnitude of E less than 8 kJ/mol and confirmed that adsorption is a physical process. Based on R^2 values and statistic error analysis (root mean square error; RMSE), the adsorption experimental data yielded excellent fits in the following isotherms order Freundlich > Langmuir > Dubinin–Radushkevich > Temkin. As can be seen Freundlich isotherm model can better describes naproxen adsorption hence the adsorption followed a multilayer process.

3.5. Adsorption mechanism

The adsorption process takes place through physical or chemical processes. Based on the results of the kinetic studies, the naproxen adsorption onto magnetic dextrin and ionomer followed pseudo-second-order model. Moreover, based on the isotherm study, adsorption followed the Freundlich model. It is known that the pseudo-second-order model is corresponding to the chemisorption process. However, the Langmuir model shows a monolayer adsorption process and the Freundlich model confirms multilayer physical sorption. Based on the above description and the experimental results, naproxen sorption is not a net physical or chemical interaction and it is along with a physicochemical sorption process. In other words, the adsorption mechanism is complex and both the chemical and physical adsorptions contribute at the same time in the adsorption process.

The composite structure contains methylene groups originated from dextrin and IL, hence it can be concluded that hydrophobic interaction between C–H groups of naproxen and the surface of adsorbent is the main reason for efficient uptake of it by the nanohybrid [55]. Naproxen also has a carboxylic acid group (Fig. 13) which converts to carboxylate at the working pH of 8. This can increase the density of electron in the naproxen structure hence increases the hydrogen bonding ability of it with the functional groups on composite surfaces. In other words, naproxen is a polar organic compound hence its adsorption efficiency tends to be increased with the increase of potential H-bonding sites on the sorbent surface (OH and N groups). Morphology of adsorbent also has a main role in the adsorption process. According to the FESEM image, as synthesized ionomer tend to be aggregated as bundles because of intramolecular hydrogen bonds of dextrin chain as well as the hydrophobic interaction between methylene groups of tertiary amine chain. Moreover, the BET data confirmed that the ionomer has a pore in its structure which can capture naproxen molecules [47]. Other main mechanism includes anion exchange between the ionomer and anionic molecules of naproxen which enhances the adsorption efficiency of the ionomer. In fact, IL on the sorbent surface contains chlorine which can be replaced with anionic species of naproxen at alkaline solution pH.

Table 8
Optimum values of variables for naproxen removal by magnetic dextrin and ionomer

	Ionomer	Magnetic dextrin
pH	8	9
Time (min)	10	8
Dosage (mg)	8	17
Ionic strength (%)	8	9
Calculated removal (%)	94	64

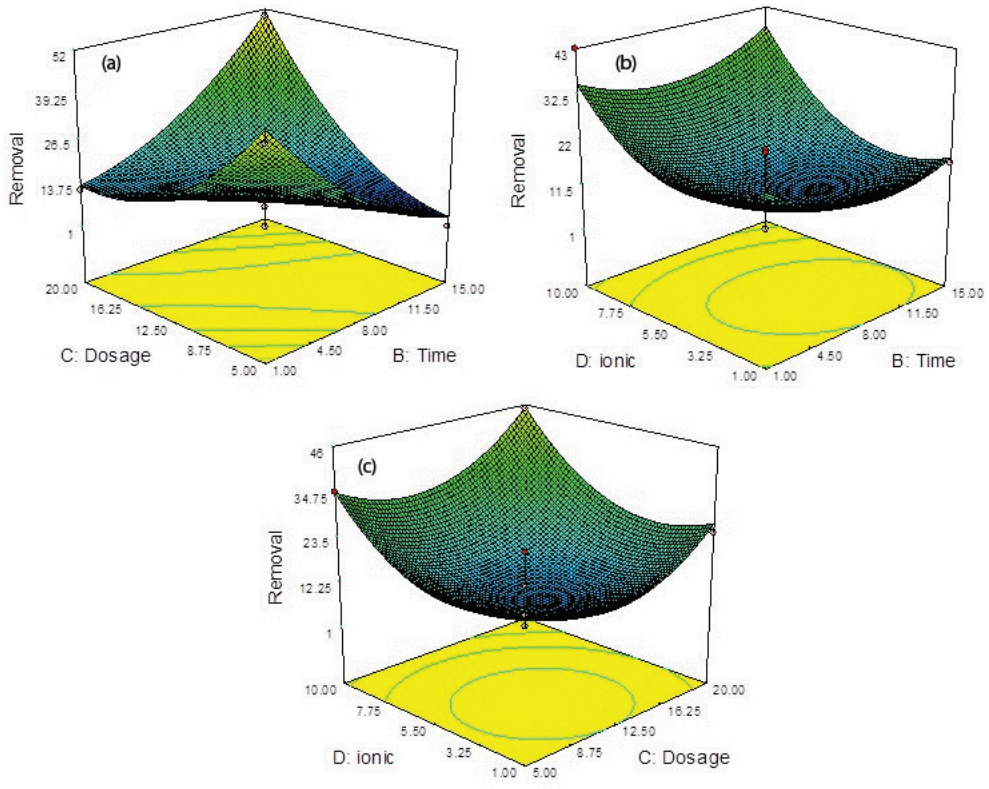

Fig. 10. 3D plots of dosage vs. time (a), ionic strength vs. time (b) and ionic strength vs. dosage (c) for naproxen removal by magnetic dextrin.

Table 9
Data of kinetic models for adsorption of naproxen using the adsorbent

Sorbent	First order			Second order			Diffusion model					Liquid film	
	Q_e(mg g^{-1})	R^2	K_1	Q (mg g^{-1})	R^2	K_2	Q (mg g^{-1})	R^2	K_p	C	R^2	K_{fd}	C
Magnetic dextrin	41.40	0.99	0.61	0.46	0.95	0.032	31.15	0.71	8.10	51.49	0.99	0.61	5.30
Ionomer	48.24	0.67	0.36	1.01	0.99	0.039	50.50	0.88	5.77	31.29	0.67	0.36	1.12

Table 10
Data of Langmuir and Freundlich isotherm for naproxen adsorption using the adsorbents

Coefficient	Freundlich		Coefficient	Langmuir	
	Magnetic dextrin	Ionomer		Magnetic dextrin	Ionomer
n	0.98	0.94	Q_m	137.0	164.0
K_f	3.49	2.64	R^2	0.92	0.91
R^2	0.91	0.98	K_L	0.051	0.024
RMSE	29.12	9.32	RMSE	36.06	25.82

Table 11
Data of D–R and Temkin isotherm for naproxen adsorption using the adsorbents

Coefficient	D–R		Coefficient	Temkin	
	Magnetic dextrin	Ionomer		Magnetic dextrin	Ionomer
B	21.82	40.97	A_T	0.49	0.24
E	0.15	0.11	R^2	0.70	0.80
R^2	0.76	0.77	B	286.27	92.57
RMSE	46.50	46.76	RMSE	60.26	57.58

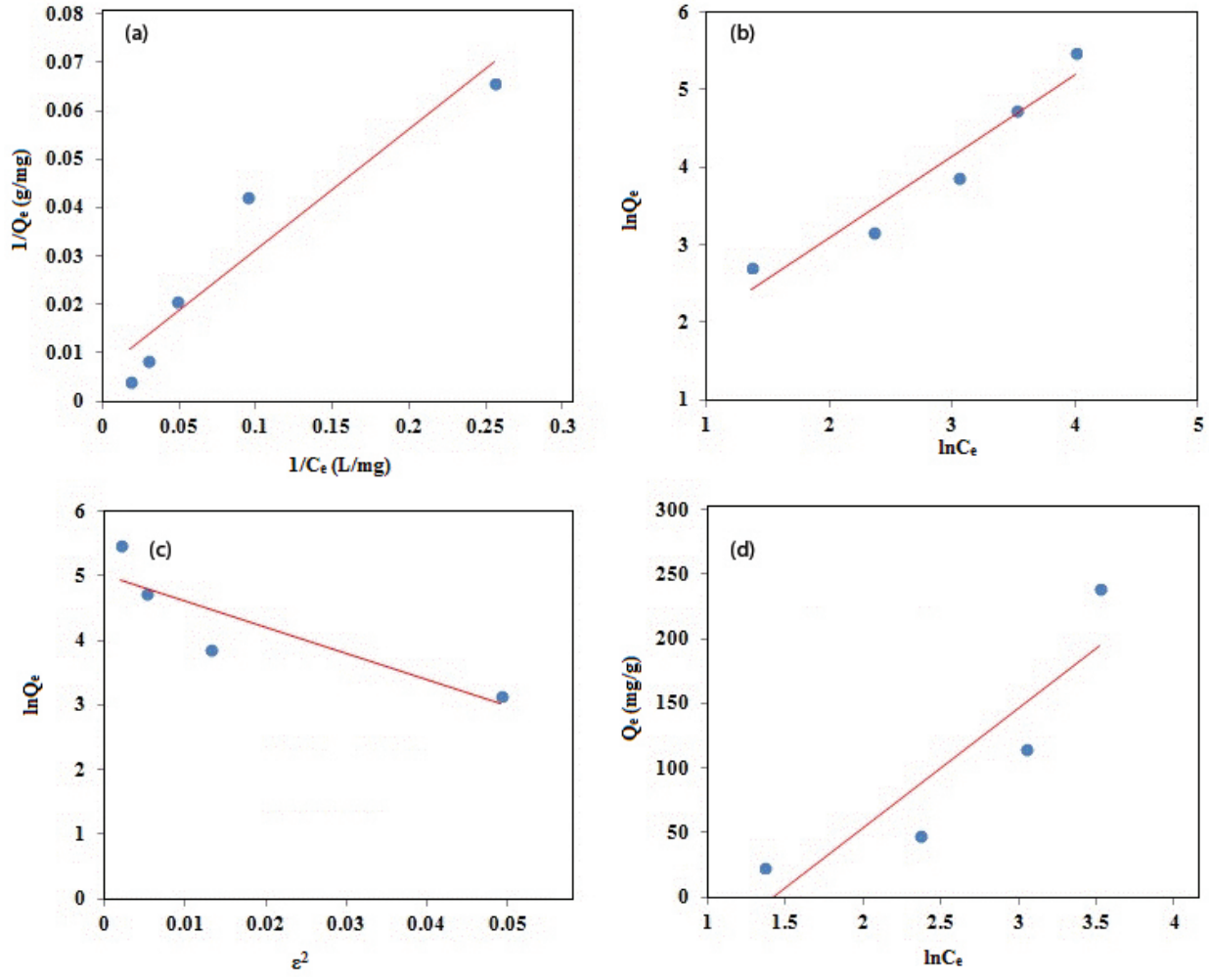

Fig. 11. Langmuir (a), Freundlich (b), D–R (c) and Temkin adsorption (d) isotherm plot of naproxen adsorption onto the ionomer.

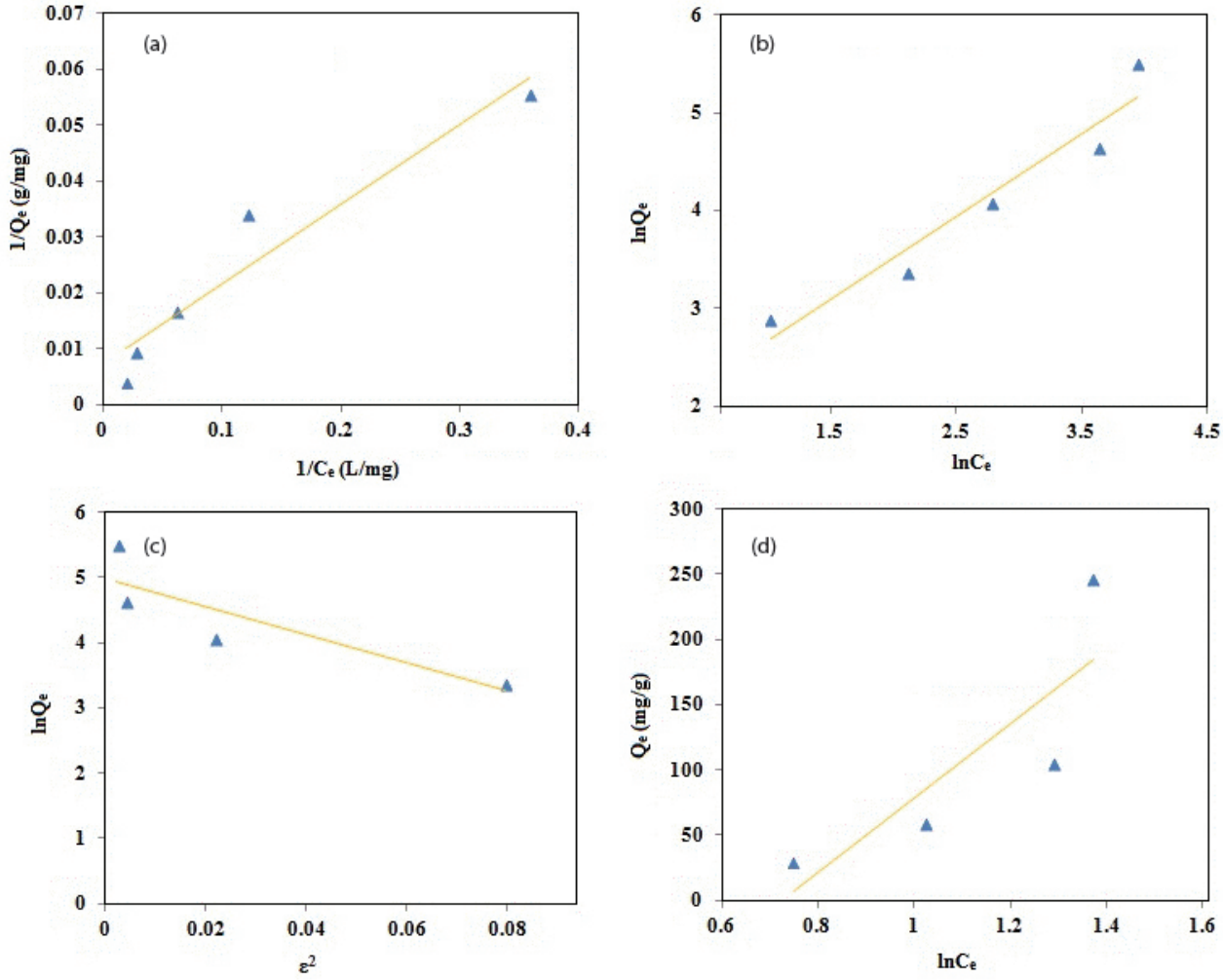

Fig. 12. Langmuir (a), Freundlich (b), D–R (c) and Temkin adsorption (d) isotherm plot of naproxen adsorption onto the magnetic dextrin.

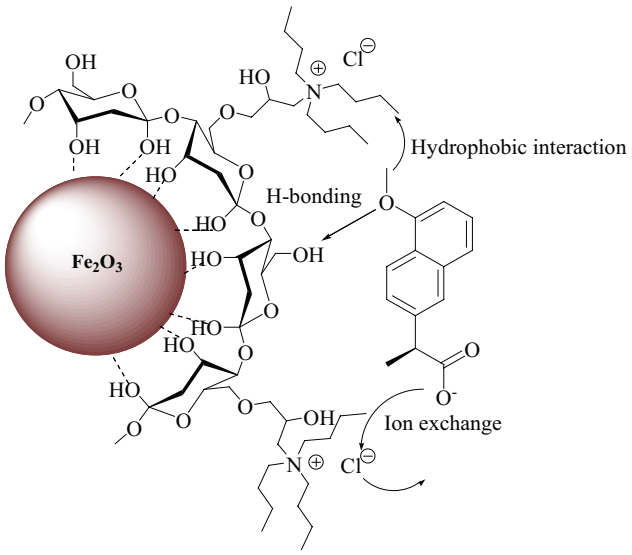

Fig. 13. A schematic illustration of the naproxen adsorption mechanism onto magnetic ionomer.

3.6. Comparison with literature

A comparative study of naproxen adsorption using magnetic dextrin and ionomer as well as with some adsorbents reported in the literature is presented in Table 12. It can be seen that the performance of ionomer is better than the magnetic dextrin as the adsorption capacity of ionomer is about 16% higher than the magnetic dextrin. This result can be assigned to the functionalization of the magnetic dextrin with IL fragment as the ionomer also can absorb naproxen molecules by hydrophobic interaction. Comparing with literature, it is obvious that the performances of the prepared sorbents are in satisfying level since they show fast equilibrium time with high adsorption capacity. Moreover, magnetic ionomer can be considered as a green biosorbent owing to the employment of IL and biopolymer in a combined structure. As a result, as synthesized sorbent appear to be a promising adsorbent for the removal of emerging micropollutants from the water. When the prices of a number of common adsorbents are compared in Table 12, the ionomer appear to be in the same range as modified clay. Moreover, it is the cheapest being

Table 12
Comparison naproxen adsorption property of prepared composite with some sorbents

Adsorbent	Maximum capacity (mg g^{-1})	Equilibrium time (min)	Price (US $ g^{-1})	Ref
Porous sugarcane bagasse	166.6	90	0.0025	[4]
Amberlie XA-4	56.84	10	5.0	[7]
β-Cyclodextrin-clay	10	120	15	[8]
Magnetic activated carbon	87.79	150	1.5	[21]
Micelle–clay	71.42	180	3.0	[56]
Imprinting polymer	3.26	10	7.0	[57]
Magnetic β-cyclodextrin	25.71	–	13	[58]
Magnetic dextrin	137	10	3.0	This work
Ionomer	164	10	4.0	This work

resin, imprinted polymer and cyclodextrin. These data indicate that ionomer is a good candidate for water treatment because of low cost, easy to preparation and green characteristic.

4. Conclusions

In this work, an efficient magnetic ionomer was developed based on Fe_2O_3 – dextrin immobilized tertiary amine and employed for naproxen adsorption. Synthesis process was based on the one-step synthesis of magnetic dextrin and its reaction with tributylamine reaction in the presence of ECH as a linker. Fabrication of IL immobilized adsorbent increases naproxen adsorption efficiency as adsorption capacity by magnetic dextrin and ionomer was 137 and 164 mg/g, respectively. This can be assigned to the anion exchange and hydrophobic interaction capability of ionomer with the analyte. Effective parameters on adsorption were optimized with RSM. It was found that naproxen adsorption showed fast equilibrium time of 10 min which followed pseudo-second-order kinetic model. Isotherm studies and error analysis revealed that adsorption of naproxen onto both adsorbents followed the Freundlich model. Prepared ionomer can be used as a water purification system as it has potential to eliminate anionic species (organic and inorganic anions) from water. Moreover it has potential to be employed for removal of pathogens from aqueous solutions. Employment as heterogeneous catalyst after anion exchange process is another potential application of the nanocomposite. Other applications that have been considered and, in some cases, test marketed on similar structures are organic viscosifiers and drilling fluids.

Acknowledgment

Support for this study by the Research Council of the University of Tehran through grants is gratefully acknowledged.

References

[1] J. Fawell, M.J. Nieuwenhuijsen, Contaminants in drinking water, Br. Med. Bull., 68 (2003) 199–208.
[2] M.H. Beyki, M. Bayat, F. Shemirani, Fabrication of core-shell structured magnetic nanocellulose base polymeric ionic liquid for effective biosorption of Congo red dye, Bioresour. Technol., 218 (2016) 326–334.
[3] H.R.J. Malakootikhah, A.H. Rezayana, B. Negahdari, S. Nasseri, Glucose reinforced Fe_3O_4@cellulose mediated amino acid: reusable magnetic glyconanoparticles with enhanced bacteria capture efficiency, Carbohydr. Polym., 170 (2017) 190–197.
[4] R.A. Reza, M. Ahmaruzzaman, Removal of naproxen from aqueous environment using porous sugarcane bagasse: impact of ionic strength, hardness and surfactant, Res. Chem. Intermed., 42 (2016) 1463–1485.
[5] C. Yu, E. Bi, Roles of functional groups of naproxen in its sorption to kaolinite, Chemosphere, 138 (2015) 335–339.
[6] G. Teijón, L. Candela, E. Sagristá, M. Hidalgo, Naproxen adsorption-desorption in a sandy aquifer matrix: characterisation of hysteretic behavior at two different temperature values, Soil Sediment Contam., 22 (2013) 641–653.
[7] K. Wieszczycka, J. Zembrzuska, J. Bornikowska, A. Wojciechowska, I. Wojciechowska, Removal of naproxen from water by ionic liquid-modified polymer sorbents, Chem. Eng. Res. Design, 117 (2017) 698–705.
[8] L. Rafati, M.H. Ehrampoush, A.A. Rafati, M. Mokhtari, A.H. Mahvi, Modeling of adsorption kinetic and equilibrium isotherms of naproxen onto functionalized nano-clay composite adsorbent, J. Mol. Liq., 224 (2016) 832–841.
[9] J. Alonso-gutierrez, D. Koma, Q. Hu, Y. Yang, Stability and removal of naproxen and its metabolite by advanced membrane wastewater treatment plant and micelle-clay complex, Clean Soil Air Water, 42 (2014) 594–600.
[10] Ç. Sarici-Özdemir, Y. Önal, Study to observe the applicability of the adsorption isotherms used for the adsorption of medicine organics onto activated carbon, Particulate Sci. Technol., 36 (2016) 1–8.
[11] C. Jung, J. Oh, Y. Yoon, Removal of acetaminophen and naproxen by combined coagulation and adsorption using biochar: influence of combined sewer overflow components, Environ. Sci. Pollut. Res., 22 (2015) 10058–10069.
[12] M.H. To, P. Hadi, C.W. Hui, C.S.K. Lin, G. McKay, Mechanistic study of atenolol, acebutolol and carbamazepine adsorption on waste biomass derived activated carbon, J. Mol. Liq., 241 (2017) 386–398.
[13] X. Li, J. Xu, R.A. de Toledo, H. Shim, Enhanced removal of naproxen and carbamazepine from wastewater using a novel countercurrent seepage bioreactor immobilized with *Phanerochaete chrysosporium* under non-sterile conditions, Bioresour. Technol., 197 (2015) 465–474.
[14] M. Sarker, J.Y. Song, S.H. Jhung, Adsorptive removal of anti-inflammatory drugs from water using graphene oxide/metal-organic framework composites, Chem. Eng. J., 335 (2018) 74–81.
[15] W. Konicki, A. Hełminiak, W. Arabczyk, E. Mijowska, Adsorption of cationic dyes onto Fe@graphite core–shell magnetic nanocomposite: equilibrium, kinetics and thermodynamics, Chem. Eng. Res. Design, 129 (2018) 259–270.
[16] X. Zhang, R. Jing, X. Feng, Y. Dai, R. Tao, J. Vymazal, Removal of acidic pharmaceuticals by small-scale constructed wetlands using different design configurations, Sci. Total Environ., 639 (2018) 640–647.

[17] E. Kurtulbaş, M. Bilgin, S. Şahin, Ş.S. Bayazit, Comparison of different polymeric resins for naproxen removal from wastewater, J. Mol. Liq., 241 (2017) 633–637.
[18] G.R. Boyd, S. Zhang, D.A. Grimm, Naproxen removal from water by chlorination and biofilm processes, Water Res., 39 (2005) 668–676.
[19] S. Álvarez-Torrellas, M. Muñoz, J.A. Zazo, J.A. Casas, J. García, Synthesis of high surface area carbon adsorbents prepared from pine sawdust-*Onopordum acanthium* L. for nonsteroidal anti-inflammatory drugs adsorption, J. Environ. Manage.. 183 (2016) 294–305.
[20] Z. Hasan, E.J. Choi, S.H. Jhung, Adsorption of naproxen and clofibric acid over a metal–organic framework MIL-101 functionalized with acidic and basic groups, Chem. Eng. J., 219 (2013) 537–544.
[21] Z. İlbay, S. Şahin, Kerkez, S. Bayazit, Isolation of naproxen from wastewater using carbon-based magnetic adsorbents, Int. J. Environ. Sci. Technol., 12 (2015) 3541–3550.
[22] J.Y. Song, S.H. Jhung, Adsorption of pharmaceuticals and personal care products over metal-organic frameworks functionalized with hydroxyl groups: quantitative analyses of H-bonding in adsorption, Chem. Eng. J., 322 (2017) 366–374.
[23] M. Hossein Beyki, F. Shemirani, M. Shirkhodaie, Aqueous Co(II) adsorption using 8-hydroxyquinoline anchored γ-Fe_2O_3@ chitosan with Co(II) as imprinted ions, Int. J. Biol. Macromol., 87 (2016) 375–384.
[24] C.T. Weber, E.L. Foletto, L. Meili, Removal of tannery dye from aqueous solution using papaya seed as an efficient natural biosorbent, Water Air Soil Pollut., 224 (2013) 1427–1438.
[25] S. Suganya, P. Senthil Kumar, A. Saravanan, P. Sundar Rajan, C. Ravikumar, Computation of adsorption parameters for the removal of dye from wastewater by microwave assisted sawdust: theoretical and experimental analysis, Environ. Toxicol. Pharmacol., 50 (2017) 45–57.
[26] E.N. Zare, M.M. Lakouraj, Biodegradable polyaniline/dextrin conductive nanocomposites: synthesis, characterization, and study of antioxidant activity and sorption of heavy metal ions, Iran. Polym. J., 23 (2014) 257–266.
[27] R. Ahmad, A. Mirza, Heavy metal remediation by dextrin-oxalic acid/cetyltrimethyl ammonium bromide (CTAB) – montmorillonite (MMT) nanocomposite, Groundwater Sustain. Dev., 4 (2017) 57–65.
[28] M. Tian, K.H. Row, SPE of tanshinones from *Salvia miltiorrhiza* bunge by using imprinted functionalized ionic liquid-modified silica, Chromatographia, 73 (2011) 25–31.
[29] J. López-Darias, J.L. Anderson, V. Pino, A.M. Afonso, Developing qualitative extraction profiles of coffee aromas utilizing polymeric ionic liquid sorbent coatings in headspace solid-phase microextraction gas chromatography-mass spectrometry, Anal. Bioanal. Chem., 401 (2011) 2965–2976.
[30] H. Olivier-Bourbigou, L. Magna, D. Morvan, Ionic liquids and catalysis: recent progress from knowledge to applications, Appl. Catal., A, 373 (2010) 1–56.
[31] M.J. Pirouz, M.H. Beyki, F. Shemirani, Anhydride functionalised calcium ferrite nanoparticles: a new selective magnetic material for enrichment of lead ions from water and food samples, Food Chem., 170 (2015) 131–137.
[32] R. Khani, S. Sobhani, M.H. Beyki, S. Miri, Application of magnetic ionomer for development of very fast and highly efficient uptake of triazo dye Direct Blue 71 form different water samples, Ecotoxicol. Environ. Saf., 150 (2018) 54–61.
[33] S. Naeimi, H. Faghihian, Application of novel metal organic framework, MIL-53(Fe) and its magnetic hybrid: for removal of pharmaceutical pollutant, doxycycline from aqueous solutions, Environ. Toxicol. Pharmacol., 53 (2017) 121–132.
[34] M. Bayat, F. Shemirani, M. Hossein Beyki, M. Davudabadi Farahani, Ionic liquid-modified Fe_3O_4 nanoparticle combined with central composite design for rapid preconcentration and determination of palladium ions, Desal. Wat. Treat., 56 (2015) 814–825.
[35] T.R. Bastami, M.H. Entezari, Sono-synthesis of Mn_3O_4 nanoparticles in different media without additives, Chem. Eng. J., 164 (2010) 261–266.
[36] A. Buntic, M. Pavlovic, K. Mihajlovski, M. Randjelovic, N. Rajic, D. Antonovic, S. Siler-Marinkovic, S. Dimitrijevic-Brankovic, Removal of a cationic dye from aqueous solution by microwave activated clinoptilolite - Response surface methodology approach, Water Air Soil Pollut., 225 (2014) 1816–1829.
[37] A. Mittal, R. Ahmad, I. Hasan, Iron oxide-impregnated dextrin nanocomposite: synthesis and its application for the biosorption of Cr(VI) ions from aqueous solution, Desal. Wat. Treat., 57 (2016) 15133–15145.
[38] X. Yang, C. Zhang, L. Wu, Nano g-Fe_2O_3-supported fluoroboric acid: a novel magnetically recyclable catalyst for the synthesis of 12-substituted-benzo[h][1,3]dioxolo[4,5-b]-acridine-10,11-diones as potent antitumor agents, RSC Adv., 5 (2015) 25115–25124.
[39] H. Yadaei, M.H. Beyki, F. Shemirani, S. Nouroozi, Ferrofluid mediated chitosan@mesoporous carbon nanohybrid for green adsorption/preconcentration of toxic Cd(II): modeling, kinetic and isotherm study, React. Func. Polym., 122 (2018) 85–97.
[40] R.M. Khafagy, Synthesis, characterization, magnetic and electrical properties of the novel conductive and magnetic Polyaniline/$MgFe_2O_4$ nanocomposite having the core-shell structure, J. Alloys Comp., 509 (2011) 9849–9857.
[41] M.H. Beyki, J. Malakootikhah, F. Shemirani, S. Minaeian, Magnetic $CoFe_2O_4$@melamine based hyper-crosslinked polymer: a multivalent dendronized nanostructure for fast bacteria capturing from real samples, Process Saf. Environ. Protect., 116 (2018) 14–21.
[42] M. Hossein Beyki, S. Ehteshamzadeh, S. Minaeian, F. Shemirani, Clean approach to synthesis of graphene like $CuFe_2O_4$@ polysaccharide resin nanohybrid: bifunctional compound for dye adsorption and bacterial capturing, Carbohydr. Polym., 174 (2017) 128–136.
[43] M. Hossein Beyki, M. Mohammadirad, F. Shemirani, A.A. Saboury, Magnetic cellulose ionomer/layered double hydroxide: an efficient anion exchange platform with enhanced diclofenac adsorption property, Carbohydr. Polym., 157 (2017) 438–446.
[44] M. Bayat, M.H. Beyki, F. Shemirani, One-step and biogenic synthesis of magnetic Fe_3O_4-fir sawdust composite: application for selective preconcentration and determination of gold ions, J. Ind. Eng. Chem., 21 (2015) 912–919.
[45] A. Dabrowski, Adsorption, from theory to practice, Adv. Colloid Interface Sci., 93 (2001) 135–224.
[46] R. Khani, S. Sobhani, M.H. Beyki, Highly selective and efficient removal of lead with magnetic nano-adsorbent: multivariate optimization, isotherm and thermodynamic studies, J. Colloid Interface Sci., 466 (2016) 198–205.
[47] M.H. Beyki, F. Feizi, F. Shemirani, Melamine-based dendronized magnetic polymer in the adsorption of Pb(II) and preconcentration of rhodamine B, React. Funct. Polym., 103 (2016) 81–91.
[48] N. Tumin, A. Chuah, Adsorption of copper from aqueous solution by Elais Guineensis kernel activated carbon, J. Eng. Sci. Technol., 3 (2008) 180–189.
[49] Y.S. Al-Degs, M.I. El-Barghouthi, A.H. El-Sheikh, G.M. Walker, Effect of solution pH, ionic strength, and temperature on adsorption behavior of reactive dyes on activated carbon, Dyes Pigm., 77 (2008) 16–23.
[50] T.K. Naiya, A.K. Bhattacharya, S.K. Das, Clarified sludge (basic oxygen furnace sludge) - an adsorbent for removal of Pb(II) from aqueous solutions - kinetics, thermodynamics and desorption studies, J. Hazard. Mater., 170 (2009) 252–262.
[51] L. You, C. Huang, F. Lu, A. Wang, X. Liu, Q. Zhang, Facile synthesis of high performance porous magnetic chitosan - polyethylenimine polymer composite for Congo red removal, Int. J. Biol. Macromol., 107 (2018) 1620–1628.
[52] K.Y. Foo, B.H. Hameed, Insights into the modeling of adsorption isotherm systems, Chem. Eng. J., 156 (2010) 2–10.
[53] N. Ayawei, A.N. Ebelegi, D. Wankasi, Modelling and interpretation of adsorption isotherms, J. Chem., 2017 (2017) 1–11.
[54] A. Dada, A. Olalekan, A. Olatunya, O. Dada, Langmuir, Freundlich, Temkin and Dubinin – Radushkevich isotherms studies of equilibrium sorption of Zn^{2+} unto phosphoric acid modified rice husk, IOSR J. Appl. Chem., 3 (2012) 38–45.

[55] B. Pan, B. Xing, Adsorption mechanisms of organic chemicals on carbon nanotubes, Environ. Sci. Technol., 42 (2008) 9005–9013.
[56] M. Awwad, F. Al-Rimawi, K.J. Dajani, M. Khamis, S. Nir, R. Karaman, Removal of amoxicillin and cefuroxime axetil by advanced membranes technology, activated carbon and micelle-clay complex, Environ. Technol., 36 (2015) 2069–2078.
[57] H.A. Panahi, A. Feizbakhsh, S. Khaledi, E. Moniri, Fabrication of new drug imprinting polymer beads for selective extraction of naproxen in human urine and pharmaceutical samples, Int. J. Pharm., 441 (2013) 776–780.
[58] H.A. Panahi, B. Tahmouresi, E. Moniri, M. Manoochehri, Synthesis and characterization of polymer brushes containing β-cyclodextrin grafted to magnetic nanoparticles for determination of naproxen in urine, Anal. Lett., 47 (2014) 2929–2938.